Soft x-ray optical constants of sputtered chromium thin films with improved accuracy in the L and M absorption edge regions

Franck Delmotte, Julia Meyer-Ilse, Farhad Salmassi, Regina Soufli, Catherine Burcklen, Jennifer Rebellato, Arnaud Jérome, Ian Vickridge, Emrick Briand, and Eric Gullikson

Citation: Journal of Applied Physics **124**, 035107 (2018); doi: 10.1063/1.5027488
View online: https://doi.org/10.1063/1.5027488
View Table of Contents: http://aip.scitation.org/toc/jap/124/3
Published by the American Institute of Physics

Articles you may be interested in

Influence of carrier diffusion on photo-Seebeck effect in zinc oxide
Journal of Applied Physics **124**, 035108 (2018); 10.1063/1.5040033

Electromagnetic properties of the Great Pyramid: First multipole resonances and energy concentration
Journal of Applied Physics **124**, 034903 (2018); 10.1063/1.5026556

Relaxation of asymmetric crystallographic tilt: In situ x-ray diffraction studies of epitaxial electrodeposition of bismuth on GaAs (110)
Journal of Applied Physics **124**, 035301 (2018); 10.1063/1.5026630

Effect of grain boundary misorientation on the apparent diffusivity in nanocrystalline aluminum by atomistic simulation study
Journal of Applied Physics **124**, 035102 (2018); 10.1063/1.5033860

Nonlinear ultrasonic response of voids and Cu precipitates in body-centered cubic Fe
Journal of Applied Physics **124**, 035104 (2018); 10.1063/1.5029368

Influence of an integrated quasi-reference electrode on the stability of all-solid-state AlGaN/GaN based pH sensors
Journal of Applied Physics **124**, 034904 (2018); 10.1063/1.5034367

Ultra High Performance SDD Detectors

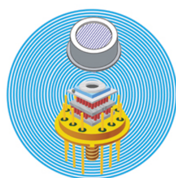
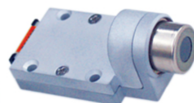

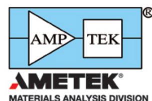

See all our XRF Solutions

JOURNAL OF APPLIED PHYSICS **124**, 035107 (2018)

Soft x-ray optical constants of sputtered chromium thin films with improved accuracy in the L and M absorption edge regions

Franck Delmotte,[1,2] Julia Meyer-Ilse,[2] Farhad Salmassi,[2] Regina Soufli,[1,3] Catherine Burcklen,[3] Jennifer Rebellato,[1] Arnaud Jérome,[1] Ian Vickridge,[4] Emrick Briand,[4] and Eric Gullikson[2]

[1]*Laboratoire Charles Fabry, Institut d'Optique Graduate School, CNRS, Universite Paris-Saclay, 91127 Palaiseau Cedex, France*
[2]*Center for X-ray Optics, Lawrence Berkeley National Laboratory, 2-400 Berkeley, California 94720, USA*
[3]*Lawrence Livermore National Laboratory, 7000 East Avenue, Livermore, California 94550, USA*
[4]*Institut des NanoSciences de Paris, 4 place Jussieu, F-75252 Paris Cedex 05, France*

(Received 2 March 2018; accepted 1 July 2018; published online 19 July 2018)

In this study, we determine with improved accuracy the complex index of refraction $n = 1 - \delta + i\beta$ of sputtered chromium thin films for photon energies ranging from 25 eV to 813 eV. These data include the first absolute measurements of the absorption fine structure near the Cr-L edge. First, we verified by combining Rutherford Backscattering Spectrometry and grazing-incidence x-ray reflectometry that the sputtered thin films were pure Cr with a density consistent with tabulated values. Then, we demonstrated that the Cr surface oxide layer remains stable when the samples are exposed to air for up to 4 years. The Cr absorption coefficient β was determined from the transmittance of free-standing Cr thin films with various thicknesses, measured at the ALS synchrotron radiation source. A model is proposed to correct the transmittance data from the spectral contamination of the source. Finally, we used the new β values, combined with theoretical and tabulated data from the literature, in order to calculate the δ values by the Kramers-Kronig relation. The improvement in the accuracy of β values is demonstrated by the f-sum rule. An additional validation of the new Cr optical constants (δ, β) is performed by comparing the simulated and experimental reflectance of a Cr/B_4C multilayer mirror near the Cr-$L_{2,3}$ edge. *Published by AIP Publishing.* https://doi.org/10.1063/1.5027488

I. INTRODUCTION

Chromium, which possesses two absorption edges (Cr-M and Cr-L) in the soft x-ray and extreme ultraviolet (EUV) spectral range, is a transition metal with numerous applications in science, industry, and metallurgy and as a magnetic material. Cr is also a material of special interest for multilayer interference coatings, which enable components in illumination and imaging systems operating in the EUV/soft x-ray range. To that end, Cr is widely used in Cr/Sc-based multilayers for a large variety of applications, such as polarizing and phase-retarding reflecting components at Cr-L and Sc-L edges,[1] condenser optics for soft x-ray microscopy,[2] mirrors for attosecond pulses,[3,4] and multilayer optics for X-ray Free Electron Lasers.[5] Other Cr-based, high-performance multilayer optics in the soft x-ray domain include Cr/B_4C,[6] Cr/V,[7,8] Cr/Ti,[9] and Cr/C.[10] High-reflectance Sc/Si multilayers operating below 27 eV have been demonstrated by introducing Cr barrier layers.[11] Cr is also a potential absorber layer material for the production of EUV lithography masks.[12] Finally, Cr thin films have been employed as under-layers to enhance adhesion between coatings and substrates and to mitigate coating stress, in optics for EUV lithography, solar physics, and astrophysics.[13–15]

The design of multilayer optics with increasingly advanced concepts (interface and capping layer engineering, tri-material structures, multi-periodic or non-periodic stacks, etc.) in the EUV and soft x-ray spectral domains requires highly accurate knowledge of material optical constants (refractive index). The most comprehensive optical constant database in this spectral range consists of the tabulated atomic scattering factors, compiled by Henke *et al.* in 1993 (the so-called "Henke tables").[16] The semi-empirical model used in these tables relies on the hypothesis of the "atomic-like" behavior of condensed matter. As the effects of the condensed state are not negligible near absorption edges and in cases where experimental data for a given material are not available in near-edge photon energy regions, the optical constants provided from Ref. 16 are not accurate in those specific regions. The optical constants of several materials of interest have been determined experimentally more recently, and an updated version of Ref. 16 is available on the Center for X-ray Optics (CXRO) website.[17]

Given the importance and wide use of Cr in science and technology mentioned above and the extensive studies of this material published in the literature, it seems therefore astonishing that experimentally determined, absolute values for the optical constants of Cr, with the near-edge fine structure resolved, have not yet been published in the vicinity of the Cr $L_{2,3}$ absorption edge. This became evident to us when we attempted to model experimental data of the reflectance of Cr/B_4C multilayers operating near the Cr $L_{2,3}$ edge, where the tabulated values for the refractive index of Cr[16] could not simulate the experimental reflective performance.[6]

One explanation for the lack of highly resolved experimental data on the refractive index of Cr in the vicinity of the $L_{2,3}$ edge may be the difficulty in preparing appropriate

samples for such measurements. For example, if the method employed is transmittance (photoabsorption) measurements, several extremely thin (10–100 nm) free-standing films are required. If reflectance measurements are employed, the microroughness on the sample surface would have to be on the order of 0.1 nm, and even in that case, accounting for the roughness would complicate the data analysis and would increase the uncertainty in the resulting refractive index values. In all measurement methodologies, and because matter is extremely absorptive in the soft x-ray region, measurements are extremely sensitive to even a few atomic monolayers of contamination on the surface or in the interior of the sample under study. Thus, the sample composition and purity need to be examined via independent methods, and the stability (aging) of the samples from the time of their preparation until the measurements needs to be verified. Even if all these requirements are satisfied, minor imperfections in the EUV/x-ray sources needed for these measurements (such as the presence of $\sim$1% spectral contamination in the Cr L edge region, discussed later in this manuscript) can influence the accuracy of the data and their subsequent analysis.

With the above challenges in mind, the main goal of this study is to determine with improved accuracy the optical constants of chromium thin films in the energy range of 25 eV–813 eV, which includes the Cr-M and Cr-L absorption edges. We discuss first the aging properties and lifetime stability of chromium sputtered thin films characterized by reflectance vs. angle measurements with hard x-rays (Cu-Kα source) and EUV radiation (synchrotron radiation source). Then, we determine the absorption coefficient of sputtered Cr thin films by transmittance measurements of self-supported films of various thicknesses, in the photon energy range from 25 eV up to 813 eV. We chose the transmittance method because it is insensitive to surface microroughness and also because any surface contamination is normalized out in the data analysis, provided that it is the same on all samples measured. Furthermore, we propose a model that allows us to correct the transmittance measurements for spectral contamination from the synchrotron radiation source. This model is then applied successfully near the Cr-L edge. Finally, we calculate the optical constants δ and β of Cr (the complex refractive index being defined as $n = 1 - \delta + i\beta$) by using the Kramers-Kronig relation. The improved accuracy of the newly determined optical constants is demonstrated by employing sum rule tests and by modeling of experimental Cr/B_4C multilayer reflectance data.

II. EXPERIMENTAL SECTION

A. Cr thin film deposition

All Cr samples studied in this manuscript were deposited by magnetron sputtering, either at CXRO or at Laboratoire Charles Fabry (LCF), with the same type of sputtering source and with very similar deposition parameters. Therefore, the conclusions from the analyses later in the manuscript can be mutually applied to samples from both depositions. This is also supported by the data presented throughout the manuscript. The deposition chamber at CXRO is a direct current (DC) magnetron sputtering machine. The magnetron sputtering deposition machine at LCF is a Plassys MP800S deposition system that has been described in previous papers.[18,19] The target was 99.99% pure Cr. The base pressure was below 10^{-6} Pa prior to deposition. During the deposition process, the Ar gas pressure was set to 0.093 Pa and the plasma discharge was established in the DC mode with a 50-mA current (a power of about 16 W). Samples deposited at CXRO include deposition on resist-coated silicon wafer substrates for the fabrication of freestanding Cr films for the transmission measurements (samples named CR1, CR2, and CR3) and deposition on silicon wafer substrates for the other characterization studies (samples named R1, R2, R3, W1, W2, and W3). Samples deposited at LCF on silicon wafer were used for the aging study (sample A), and a few samples were also used for Rutherford Back Scattering (RBS) characterization.

B. Grazing incidence X-ray reflectometry (GIXR)

Grazing incidence X-ray reflectometry (GIXR) was performed with a commercial diffractometer (BRUKER® Discover D8) equipped with a Cu Kα radiation source (wavelength $\lambda = 0.154$ nm), a collimating Göbel mirror, a rotary absorber, Soller and divergence slits, and a scintillator. The reflectance curve is obtained by scanning the grazing incidence angle while tracking the reflected beam (θ-θ scan configuration). The mechanical angular accuracy and angular resolution are better than 0.01°. We fit the GIXR data with a genetic algorithm by using the program Leptos® in order to deduce several sample parameters: layer thickness, material density, and average interfacial roughness.

C. EUV/soft x-ray reflectance and transmittance

The EUV/soft x-ray reflectance and transmittance measurements discussed in Secs. III B, IV and V, were performed at beamline 6.3.2. of the Advanced Light Source (ALS) synchrotron at LBNL. Beamline 6.3.2. has a grating monochromator with a fixed exit slit; its general characteristics have been described in detail earlier.[20,21] A set of filters of various materials (with each filter selected specifically for each photon energy range) is used for wavelength calibration and 2nd harmonic and stray light suppression. For higher-order harmonic suppression, an "order suppressor" consisting of three mirrors at a variable grazing incidence angle (depending on energy range) and based on the principle of total external reflection is used in addition to the filters. The measurement chamber allows translation of the sample in three dimensions, tilt in two dimensions, and azimuth rotation of the sample holder. The available detectors include various photodiodes and a CCD camera (the latter for sample alignment), which can be rotated by 360° around the axis of the chamber. During the measurements discussed in this manuscript, the signal was collected with either a GaAsP or a Si photodiode detector with an angular acceptance of 1° and 2.4°, respectively. The ALS storage ring current was used to normalize the signal against the storage ring current decay. The base pressure in the measurement chamber was 10^{-7} Torr.

The reflectance measurements at 150 eV discussed in Sec. III B were obtained with the 200 lines/mm

monochromator grating, a B filter for 2nd-harmonic, and stray light suppression, with the order suppressor consisting of three C-coated mirrors at a grazing incidence angle of 8° and the GaAsP photodiode. The photon energy was calibrated on the $L_{2,3}$ absorption edge of a Si filter.

The transmittance measurements around the C-K edge discussed in Sec. III B were obtained with the 600 lines/mm monochromator grating, a Ti filter for 2nd-harmonic, and stray light suppression, with the order suppressor consisting of three Ni-coated mirrors at a grazing incidence angle of 8° and the Si photodiode. The photon energy was calibrated on the K absorption edge of a B filter.

For the transmittance measurements discussed in Secs. IV and V, three gratings (80, 200, and 1200 lines/mm) were used in the monochromator to access the photon energy range from 25 to 813 eV. Photon energy calibration was based on the absorption edges of a series of filters (Al, Si, Ti, and Cr) with a relative accuracy of 0.011% rms and with a repeatability of 0.007%. For 2nd harmonic and stray light suppression, a series of transmission filters (Mg, Al, Si, Be, B, Zr, C, Ti, Cr, Co, and Cu) was used. The order suppressor consisted of three C- or Ni-coated mirrors at a grazing incidence angle ranging from 20° to 6°, depending on the photon energy range. At photon energies above 563.5 eV, a 2 mm-diameter pinhole was used in front of the reflectometer chamber to block scattered light from the 1200 lines/mm monochromator grating. The signal was collected with the Si photodiode at 25–563.5 eV and the GaAsP photodiode at 563.5–813 eV.

More specifically, the transmittance measurements in the vicinity of the Cr-L edge discussed in Sec. V were obtained with the 1200 lines/mm monochromator grating, a Co filter for 2nd-harmonic, and stray light suppression, with the order suppressor consisting of three Ni-coated mirrors at a grazing incidence angle of 6°, the 2 mm-diameter pinhole, and the GaAsP photodiode. The photon energy was calibrated on the $L_{2,3}$ absorption edge of a Cr filter.

The simulations and/or fits of the reflectance and transmittance data were made with the IMD software.[22]

D. RBS measurements

The absolute areal density (atoms/cm^2) and impurity content of Cr thin films deposited on silicon wafer were determined by RBS on the SAFIR platform of Sorbonne Université (France). A 15-nA, 1-mm beam of 2 MeV $^4He^+$ ions was directed at normal incidence onto the samples, and backscattered ion spectra were obtained with a semiconductor particle detector at a scattering angle of 165°. For the absolute measurements of areal density, we used a reference sample of Bi atoms implanted into Si ($5.66 \times 1015 \pm 2\%$ Bi atoms/cm^2).[23] RBS analyses determine the total number of atoms per unit surface area. The ratio of this amount to the thin film physical thickness (deduced from GIXR) gives the density of the thin film.

III. CHROMIUM THIN FILMS

A. Composition and aging

The reflectance of several Cr samples was measured at ALS beamline 6.3.2 a few weeks after deposition, which is the period of time that elapsed between the fabrication of the samples and the measurements of transmittance discussed later in this manuscript. The reflectance vs. angle scan, obtained at a photon energy of 150 eV on sample W1 (~50 nm thick Cr layer deposited on a silicon wafer), is plotted in Fig. 1. The best fit of these data (also plotted in Fig. 3) is obtained with a thin layer of Cr_2O_3 on top of the Cr layer. The fitted thickness of the Cr_2O_3 and Cr layers is 0.91 nm and 49.36 nm, respectively. The presence of an oxide layer with a thickness in the range of 0.8 nm to 1.3 nm has been confirmed by measurements on other samples. The formation of a Cr_2O_3 layer on the Cr surface exposed to air has already been reported by several authors (see, for instance, Refs. 24 and 25).

The presence of the chromium oxide layer on the Cr thin film surface raises the question of its stability over time and its influence on the total thickness (Cr + Cr_2O_3). To answer this question, we have performed an aging study on several samples. The samples were stored in Fluoroware™ boxes under air atmosphere in a cleanroom environment. We measured GIXR 3 samples (named R1, R2, and R3) after 9 to 12 months of aging. We have plotted in Fig. 2 a typical GIXR scan measured on sample R1 (with a Cr thickness similar to sample W1). This measurement confirms the presence of a Cr oxide layer on top of this ~1-year-old sample. Indeed, the amplitude modulation in the "Kiessig" fringes is due to the presence of a top oxide layer. The position of the amplitude minimum (around 3.1° in Fig. 2) allows us to determine precisely the thickness of this top oxide layer (typically within ±0.05 nm). The fit of these experimental data is also plotted in Fig. 2. We have introduced a top chromium oxide layer (Cr_2O_3) in the fitting model. We have also introduced a silicon native oxide layer (~2 nm thick) on top of the substrate because the silicon substrates were not deoxidized prior to deposition. Thus, the fitting layer model is the Cr_2O_3/Cr/SiO_2/Si-substrate. The hydrocarbon contamination layer that may be present on the sample surface is not taken into account in our model because GIXR spectra are not sensitive to such a layer. The fitted Cr_2O_3 thickness is about 1.5 nm, and the surface roughness is around 0.8 nm. Notice that the GIXR roughness parameter includes all interface imperfections and does not necessarily correspond to the topological roughness value.[22] The fitted Cr_2O_3 density

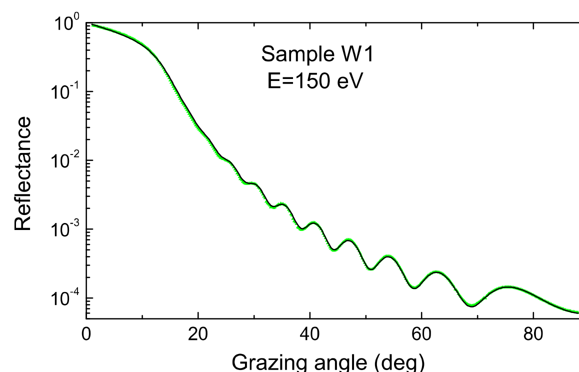

FIG. 1. Reflectance spectra (data = green triangles and fit = black line) of a 50-nm-thick Cr layer deposited on a silicon wafer (sample W1), measured 71 days after deposition at a photon energy of 150 eV at ALS beamline 6.3.2. Details of the fitting model are given in the text.

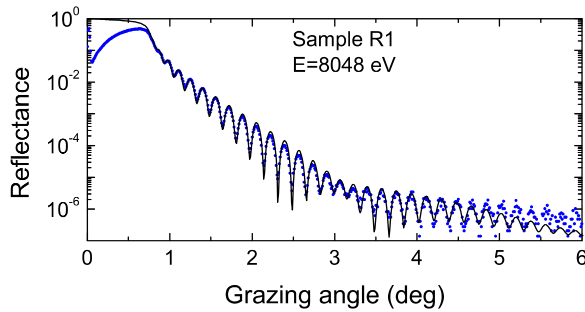

FIG. 2. GIXR spectra of a 50 nm thick Cr layer deposited on a silicon wafer (sample R1). Shown are experimental data (blue dots) measured 341 days after Cr deposition and fit (black line). Details of the fitting model are given in Table I and in the text.

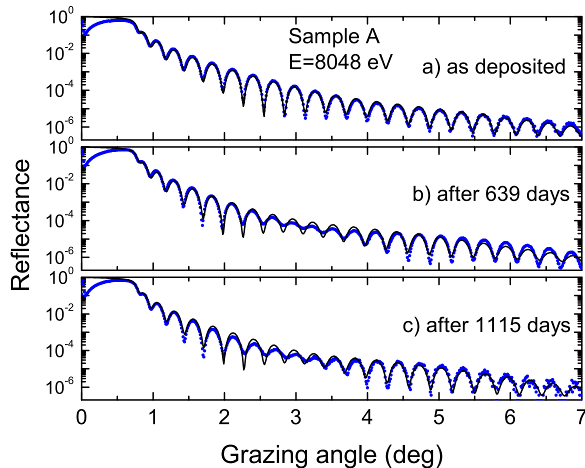

FIG. 3. Experimental GIXR spectra (blue dots) of sample A (MP14023): (a) as deposited, (b) 639 days after deposition, and (c) 1115 days after deposition. The fits of these data are also plotted (black line). Details of the fitting model are given in the text and in Table I.

(5.26 g/cm^3) is very close to the Cr_2O_3 nominal density (5.21 g/cm^3). The GIXR measurements of the samples R2 and R3 (not shown here) present similar trends as sample R1. The fitted thicknesses for samples R2 and R3 (see values in Table I) show that the oxide layer thickness on aged samples does not depend on the Cr layer thickness (for thicknesses in the range 20 nm to 50 nm and aging time of 9 to 12 months).

We also present in Fig. 3 the typical evolution of GIXR scans on a Cr thin film sample (sample A) over a period of 3 years. All data have been fitted with a Cr_2O_3 oxide layer (density = 5.21 g/cm^3) on top of the Cr layer. All the fits are achieved with the nominal density for the Cr layer (7.19 g/cm^3).

The fit of the as-deposited sample [Fig. 3(a)] gives a Cr_2O_3 thickness of 1.3 nm. The fitted Cr_2O_3 thickness for the scans measured after 639 days and 1115 days [Figs. 3(b) and 3(c), respectively) is about 1.6 nm. This indicates that the Cr_2O_3 thickness remains stable over time after a slight growth in the initial stage.

Moreover, the total thickness (i.e., the sum of Cr thickness and Cr_2O_3 thickness) remains essentially constant over time. The fitted values of the total thickness are 29.21 nm, 29.27 nm, and 29.12 nm for Figs. 3(a), 3(b), and 3(c), respectively. Thus, the variation of the total thickness is only 0.1 nm after 3 years of aging.

Finally, GIXR measurements on other Cr samples (not shown here) show that the Cr_2O_3 thickness on as-deposited samples is in the range of 0.9 nm to 1.3 nm and that its thickness remains less than 2 nm after up to 4 years of aging. Moreover, the total thickness of the film remains constant to within 0.2 nm during and after the Cr oxide formation process.

The Cr thin film aging results presented above are summarized in Table I. It is demonstrated that the oxide thickness on the surface of Cr thin films exposed to air is stable after several months after deposition, the oxide thickness remains below 2 nm, and it is independent of the Cr film thickness.

Samples R1, R2, and R3 (Table I) have been characterized by Rutherford Backscattering in order to determine the composition and density of the Cr layers. These samples were measured by GIXR a few days before RBS analysis and fitted with a model including Cr oxide (Cr_2O_3) on top of the Cr layer (an example is given in Fig. 2 for sample R1).

We have plotted in Fig. 4(a) the RBS spectra measured on sample W1. The peak at ~1450 keV corresponds to He+ particles backscattered on Cr atoms, and the signal at energy below 1100 keV corresponds to the backscattering on the Si substrate. The absence of the measurable signal in the other energy ranges shows that contamination in Cr thin films is negligible or at least lower than the sensitivity of the RBS technique. We have estimated for instance by simulation with the software SIMNRA[26] that the presence of 0.5% of Ar contamination in the Cr layer should have been detectable in our experimental conditions.

The integral of the "Cr" peak, after normalization with the measurement on a reference sample, allows us to determine the total amount of Cr atoms, i.e., the Cr atomic density in at/cm^2.[27]

We have plotted in Fig. 4(b) this Cr atomic density versus the total thin film thickness (Cr plus Cr_2O_3 layers) for the 3 samples (R1, R2, and R3). A linear fit of the data is also plotted. The very good alignment of the data points shows

TABLE I. Cr thin film aging results.

Sample	Days after deposition	Cr thickness (nm)	Cr_2O_3 thickness (nm)	Total thickness (nm)	Cr roughness (nm)	Cr_2O_3 roughness (nm)
W1	71	49.36	0.91	50.27	0.74	0.60
R1	341	47.2	1.56	48.76	0.41	0.73
R2	286	27.12	1.56	28.68	0.45	0.55
R3	285	17.32	1.53	18.85	0.42	0.55
A	0	27.9	1.31	29.21	0.39	0.45
A	639	27.66	1.61	29.27	0.36	0.54
A	1115	27.56	1.56	29.12	0.30	0.54

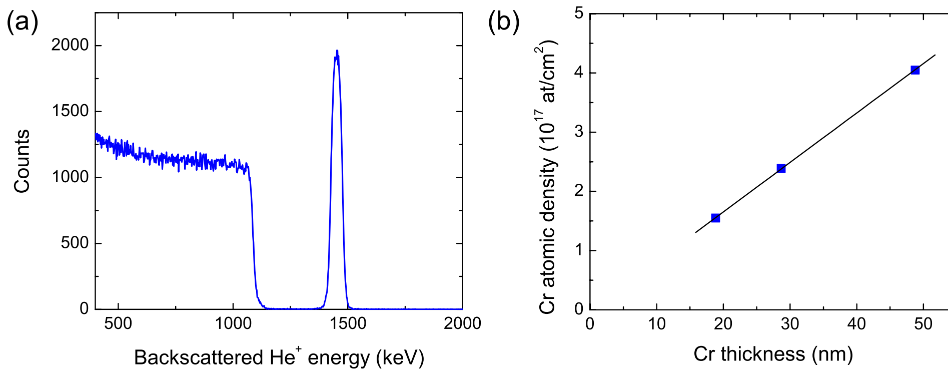

FIG. 4. (a) RBS spectra measured on sample R1 and (b) Cr atomic density versus Cr thickness measured on samples R1, R2, and R3.

that the composition of the Cr film is uniform within the depth. The offset of the linear fit is less than 2×10^{15} at/cm^2 (i.e., less than one atomic layer of Cr). This very low value confirms the consistency of our GIXR fitting model. We can determine the Cr layer density from the slope of the linear fit and the atomic mass of Cr. We found a density of 7.2 ± 0.2 g/cm^3, which is compatible with the tabulated values for pure Cr (7.18 to 7.2 g/cm^3 from Ref. 28). A similar density has been measured on Cr samples deposited at LCF with 30 nm and 60 nm Cr thicknesses (not shown here). These density values are in good agreement with the Cr density value of 7.19 g/cm^3 used in our GIXR and 150 eV data model.

B. Preparation and characterization of freestanding Cr samples

The determination of the Cr thickness for the freestanding samples was achieved by measuring reflectance vs angle at ALS beamline 6.3.2 at fixed photon energy (E = 150 eV). It appears that these measurements were less sensitive to the relatively high roughness introduced by the resist layer (about 2 nm rms) than the GIXR scans. For the latter, the Kiessig fringes are hardly visible when Cr is deposited on resist.

The Cr thickness was determined by measuring either the Cr-on-resist sample (when possible) or the Cr witness sample. The witness sample is deposited in the same deposition run on a Si wafer substrate (without resist). The experimental reflectance data used to determine the thickness of the Cr transmission samples are plotted in Figs. 5(a) and 5(b). In order to reduce the number of fitting parameters, we choose a simple model without the oxide layer on top to fit the data. The fitted thickness of Cr on sample W1 with this single layer model (Cr on the Si substrate) is 50.24 nm. Note that this value is almost identical to the total thickness (i.e., the sum of Cr and Cr_2O_3 thicknesses) obtained with the more complex model plotted in Fig. 1 (see Table I). Thus, we can consider that the Cr thickness fitted with the single layer model corresponds to the total thickness of Cr and Cr oxide.

For all samples, the fitted Si substrate roughness ranges between 0.3 nm and 0.4 nm. Concerning the 3 samples deposited on resist (named CR3, CR4, and CR5; see Table II), the fits give a resist thickness between 40 nm and 60 nm and a resist roughness in the range 1.7 nm to 2 nm (depending on the sample). The fitted thickness and surface roughness for each of the Cr layers are given in Table II for the 6 samples plotted in Figs. 5(a) and 5(b). For one deposition run, we measured both the Cr-on-resist sample (CR3) and its witness sample (W3) in order to confirm that the Cr thickness is the same in both cases. The fits for these 2 samples are superimposed with the experimental data in Fig. 5(b). The fitted Cr thicknesses are 29 nm and 28.96 nm for samples CR3 and W3, respectively. This result shows that the witness samples are representative of their corresponding transmission samples and that we can use the witness samples to determine the Cr thickness.

The values of the Cr thickness listed in Table II, determined by reflectance measurements at 150 eV on transmission samples, are consistent with those determined by fitting GIXR measurements on witness samples (not shown here). The difference between fits to both measurements is less than 0.2 nm, which also represents the estimated thickness accuracy from fits at 150 eV, for all samples.

After deposition of the Cr layers on the resist-coated Si wafers, a washer with a 3 mm diameter aperture was glued on

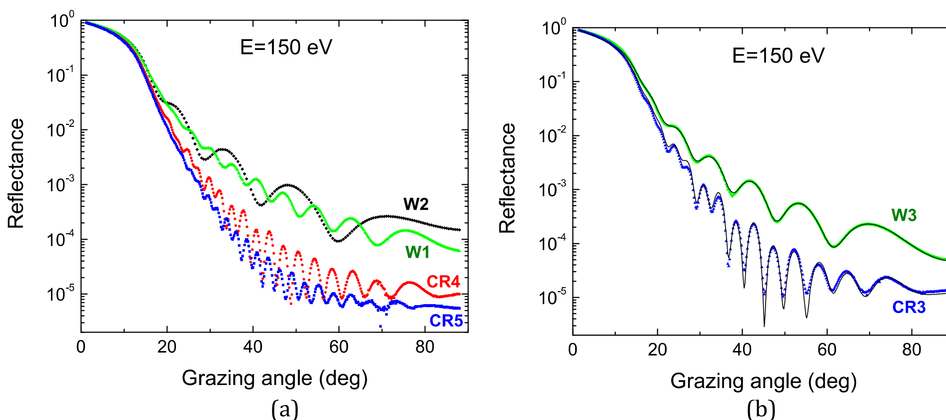

FIG. 5. Reflectance angular scan measured at fixed photon energy (E = 150 eV) at ALS beamline 6.3.2. Shown are samples (a) W1 (green triangles), W2 (black diamonds), CR4 (red circles), and CR5 (blue squares) and (b) W3 (green diamonds) and CR3 (blue triangles), with associated fits (black lines).

TABLE II. Thickness and surface roughness of Cr samples.

Sample	Substrate	Total thickness (nm)	layer roughness (nm)
W1	Silicon	50.16	0.76
W2	Silicon	19.56	0.69
W3	Silicon	28.96	0.73
CR3	Resist on silicon	29	1.78
CR4	Resist on silicon	40.86	1.81
CR5	Resist on silicon	59.93	2.05

the Cr films. Then, the resist layer was removed by chemical etching and the freestanding Cr films remained attached to the washers, which allows easy handling of the freestanding samples. After obtaining the freestanding Cr films, we used a UV-ozone lamp in order to remove carbonaceous resist residues.[29] First, we optimized the UV-ozone exposure time by measuring the soft x-ray transmission on the freestanding Cr samples, exposed to different amounts of time. More specifically, we measured the transmission spectra around the C-K absorption edge after different UV exposure times, from 0 to 36 min with 6-min steps. In order to normalize these data, we simulated the transmission spectra of a pure Cr layer with a thickness corresponding to each sample. Then, we subtracted the experimental transmission spectra from the simulated ones. We have plotted in Fig. 6 these normalized spectra that provide an estimation of the presence of residual resist. Peaks corresponding to the presence of carbonaceous components clearly appear between 285 eV and 290 eV on the spectra measured prior to UV exposure. These peaks are significantly reduced when the sample is submitted to UV exposure. After 30 min of exposure time, the signal does not evolve any more. Moreover, we have checked by looking at the transmission around the O-K edge (not shown here) that the oxygen content does not increase significantly after 30 min of UV-ozone exposure. Consequently, we selected 30 min as the optimal UV-ozone exposure time for all freestanding samples.

IV. TRANSMITTANCE OF Cr FREESTANDING THIN FILMS

The normal incidence transmittance of 5 freestanding Cr samples with thicknesses corresponding to those given in Table II has been measured from 25 eV to 813 eV at ALS beamline 6.3.2. The experimental data corresponding to samples CR1 (19.56 nm thick), CR4 (29 nm thick), and CR5 (59.93 nm thick) are plotted in Fig. 7 (for more clarity, we did not plot the transmittance spectra of samples CR2 and CR3 that range in between the 3 spectra displayed in Fig. 7). The main features that appear on all spectra are associated with the Cr-$M_{2,3}$ and Cr-$L_{2,3}$ absorption edges. We took special care to ensure that the dark current and noise signals on the detector remain well below the transmittance signal level in the entire spectral range. The high dynamic range and good spectral purity of ALS beamline 6.3.2 allow us to measure transmittance values below 10^{-3} in the low energy region (around the Cr-$M_{2,3}$ edge). Faint features (not visible in Fig. 7) are also present on all spectra around the C-K and O-K absorption edges (about 285 eV and 531 eV, respectively). These features are associated with the presence of C and O as contamination and oxide surface layers, and they appear to be very similar for the 5 freestanding samples. Moreover, the shape and position of the O-K edge features are very similar to XANES[30] or NEXAFS[31] spectra measured on Cr_2O_3 particles, thus further validating the presence of surface oxide as Cr_2O_3, used in our models in Sec. III.

At each photon energy (E), the transmittance versus Cr thickness (x) can be expressed as an exponential decay

$$T(E,x) = T_0(E)\exp(-x\alpha(E)), \qquad (1)$$

where α (E) is the linear absorption coefficient (nm^{-1}) of Cr. If the oxide surface layers are the same for all samples and x is the thickness of pure Cr, then $T_0(E)$ corresponds to the transmittance of the oxide surface layer. Following our results on the study of Cr oxide layers (see Sec. III), we consider that the surface oxide layer (Cr_2O_3) is about 1.5 nm thick on both sides of the Cr freestanding thin film (see Fig. 8). In consequence, the Cr layer thickness (x) can be calculated by subtracting 3 nm from the total layer thickness reported in Table II.

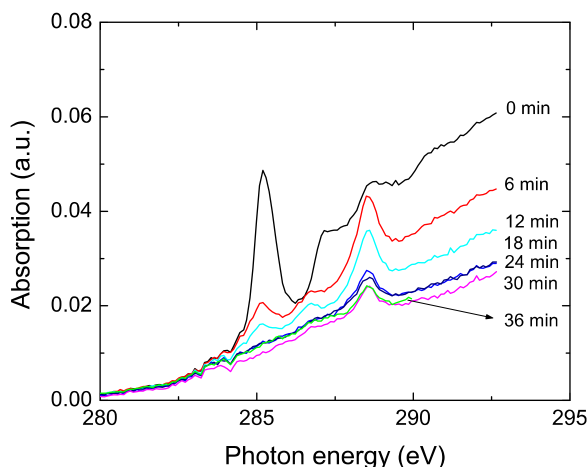

FIG. 6. Absorption spectra around the C-K edge measured on freestanding Cr samples with different UV-ozone exposure times, from 0 to 36 min.

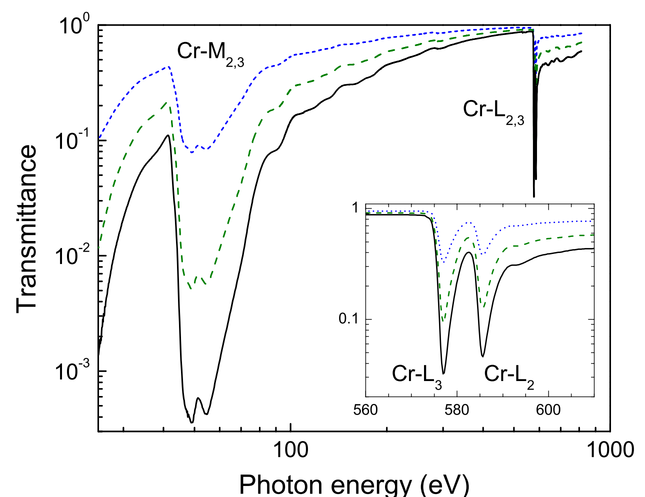

FIG. 7. Transmittance spectra vs. photon energy measured on ALS 6.3.2 beamline for samples CR1 (blue short dash), CR4 (green dash), and CR5 (dark solid line). The inset shows a detail of the Cr-$L_{2,3}$ spectral region with the photon energy on a linear scale.

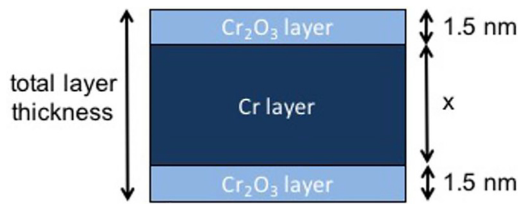

FIG. 8. Schematic of the Cr freestanding thin film.

For each photon energy E in the range 25 eV to 813 eV, we have fitted the transmittance versus thickness in order to determine $\alpha(E)$ and $T_0(E)$ using a least squares regression model. We have plotted in Fig. 9 the transmittance versus thickness for 5 different photon energies, in order to illustrate this process. The fits of each set of data are plotted as straight lines (with the transmittance plotted on a logarithmic scale), the slope and intercept of which define the values of α and T_0, respectively. Thus, with this method, the presence of any surface contamination (T_0) is normalized out of the data, provided that the surface contamination is the same on all samples, as is the case here.

The values of T_0 determined by these fits are plotted in Fig. 10. We have also plotted for comparison of the theoretical transmittance of a 3 nm-thick Cr_2O_3 layer, which corresponds to our initial hypothesis of oxide layer thickness (see Fig. 8). A 1 nm-thick C layer was added on top of the Cr_2O_3 layer in the simulation, in order to take into account a contamination layer. As the simulation was performed with tabulated atomic scattering factors,[16] we do not expect to reproduce the fine structure that appears around absorption edges nor the potential shift in absorption edge energies due to the chemical environment (as for the O-K edge in Cr_2O_3 for instance). Nevertheless, one can notice a very good overall agreement between the simulation and the fitted values of T_0. This result is consistent with our measurements of the oxide thickness in Sec. III and re-confirms the validity of our model for the oxide on the Cr samples.

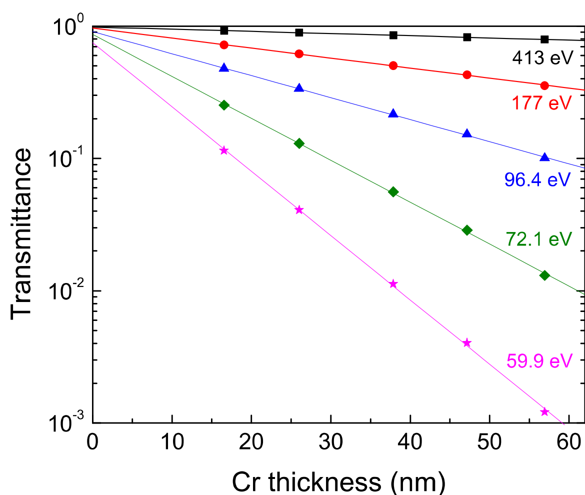

FIG. 9. Transmittance as a function of the Cr thickness for several photon energies ranging from 59.9 eV to 413 eV. The lines are fits of the data points with the exponential decay function [see Eq. (1)]. The slope and intercept of the regression line for a given photon energy define the values of α and T_0 at this energy, respectively.

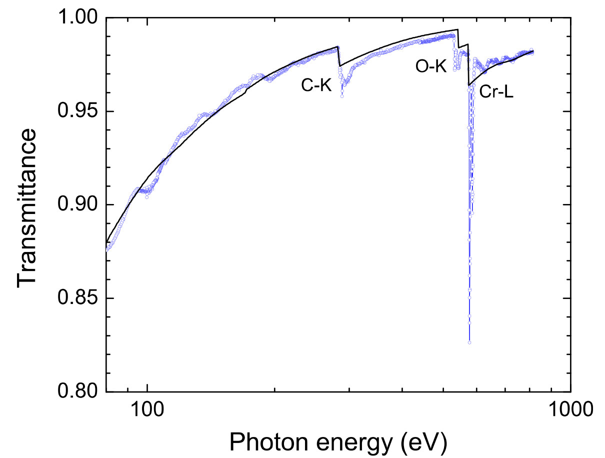

FIG. 10. Values of T_0 determined by fits of our transmission measurements (blue circles) from 80 eV to 813 eV. We also plot for comparison the simulated transmittance of a 3 nm thick Cr_2O_3 layer with 1 nm C on top (black line).

We also calculated the coefficient of determination (defined as the square of the Pearson correlation coefficient) for each fit. This factor ranges between 0.999 and 1 for most of the data points in the energy range from 25 eV to 813 eV. The only fits with a coefficient of determination lower than 0.999 were in the Cr L edge spectral region (from 574 eV to 590.4 eV). The plots of transmittance as a function of the Cr thickness in this spectral region (not shown here) show that the transmittance of the thickest sample deviates from the theoretical exponential decay (it is higher than expected). We have attributed this effect to the fact that the source is not perfectly monochromatic. Indeed, as we will demonstrate below, even a very low spectral contamination may contribute significantly to the signal in this spectral region. We propose hereafter a simple model that allows us to determine the level of spectral contamination and to calculate the correct α values close to the Cr L edge.

V. MODEL FOR THE CORRECTION OF SPECTRAL CONTAMINATION

We consider here that the incident beam is not fully monochromatic but contains a small amount of spectral contamination. The intensity of the incident beam at a selected energy E is

$$I_0(E) = I(E) + I_{sc}(E), \tag{2}$$

where I(E) is the intensity of the part of the beam that is monochromatic and $I_{sc}(E)$ is the intensity of the spectral contamination (that depends *a priori* on the selected energy E).

The spectral contamination may originate from residual higher harmonics or diffuse scattering of the monochromator.

We can write the measured transmittance as the sum of two terms

$$\begin{aligned} T(E, x) = {} & T_0(E)\kappa \exp(-x\alpha(E)) \\ & + T_{sc}(E)(1-\kappa)\exp(-x\alpha_{sc}), \end{aligned} \tag{3}$$

where κ represents the ratio of I(E) to $I_0(E)$, T_{sc} the average transmittance of the oxide surface layer for the spectral

contamination, and α_{sc} the slope of the exponential decay corresponding to the spectral contamination. If $\kappa = 1$, then the incident beam is fully monochromatic and Eq. (3) reduces to Eq. (1). A similar formalism has been earlier proposed independently in Ref. 32 to take into account the contribution of the monochromator 2nd harmonic (which was higher than 10% in their case).

In general, κ is close to 1, and the second term in Eq. (3) is negligible. However, in some specific cases, if, for example, α(E) is much higher than α_{sc}, the spectral contamination term may become predominant as the film thickness increases. This is the case in the vicinity of the Cr L edge where α(E) reaches high values.

In order to evaluate the effect of the spectral contamination on the determination of the Cr absorption coefficient in the Cr L edge spectral range, we measured the transmittance of six freestanding Cr samples with thicknesses ranging from 30 nm up to 300 nm. We plotted in Fig. 11 the data measured at two photon energies (575.33 eV and 583.45 eV). The evolution of the transmittance as a function of the film thickness clearly shows two slopes (on a logarithmic scale), which is consistent with the model depicted by Eq. (3). The fitting results of these data using the model of Eq. (3) are also plotted in Fig. 11, and the fitting parameters are given in Table III. In order to reduce the number of free parameters, we supposed that, for a given energy, T_0 and T_{sc} are equal. We can see in Fig. 11 that the spectral contamination model is in very good agreement with the experimental data.

This model was then applied to all experimental data for photon energies ranging from 574 eV to 590.4 eV (Cr L edge region). The effect of spectral contamination on the determination of the Cr absorption coefficient was found to be negligible (typically $< 1\%$) for the rest of the spectrum outside the Cr-L edge region, including the Cr-M edge region.

VI. DETERMINATION OF Cr OPTICAL CONSTANTS

The α values determined by fits of our transmission measurements from 25 eV to 813 eV, including spectral contamination correction in the Cr-L edge region, are plotted in Fig. 12. α values calculated from tabulated data of Ref. 16 are plotted for comparison. The overall agreement is quite good for photon energies above 100 eV, except in the Cr L edge region where our measurements demonstrate sharp resonance features and detailed near-edge fine structure (see the inset in Fig. 12). At energies below 100 eV, in the Cr-M edge region, the values that we determined are quite different from tabulated data.[16] Specifically, we found the absolute values of α to be higher than previous measurements on evaporated Cr,[33] which reported a maximum value of about 0.1 nm^{-1} around the Cr-M edge with an uncertainty of 20%. There is, however, good agreement in the position of the 2 maxima on the Cr-M edge between our measurements and Ref. 33.

To determine the complex refractive index $n = 1 - \delta + i\beta$ of Cr, we first calculate the absorption β from the values of α that we have obtained in Fig. 12 by using the following equation:

$$\beta(E) = \lambda\,\alpha(E)/4\pi. \quad (4)$$

The δ values, which belong to the dispersive portion of the refractive index, are calculated by means of the Kramers-Kronig relation given in the following equation:[34]

$$\delta(E) = -\frac{\pi}{2}\,P\int_0^{\infty}\frac{E'\beta(E')}{E'^2 - E^2}\,dE', \quad (5)$$

where P denotes the Cauchy principal value of the integral.

The β values used in Eq. (5) consist of the following compilation of data: (i) theoretical data simulated using the

TABLE III. Fit parameters for transmittance data plotted in Fig. 11 [see Eq. (3)].

Energy (eV)	κ	T_0 (=T_{sc})	α (nm^{-1})	α_{sc} (nm^{-1})
575.33	0.990	0.946	0.06321	0.00298
583.45	0.989	0.954	0.05026	0.00503

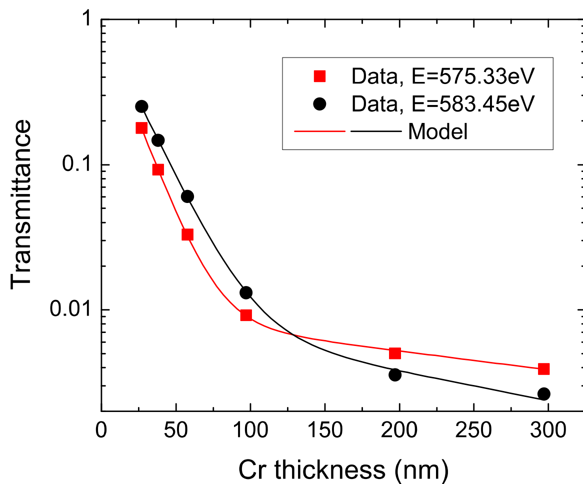

FIG. 11. Experimental transmittance as a function of the Cr thickness for photon energies of 583.45 eV (black circles) and 575.33 eV (red squares). The lines correspond to the fit of the data with the spectral contamination model [Eq. (3)]. Fit parameters are given in Table III.

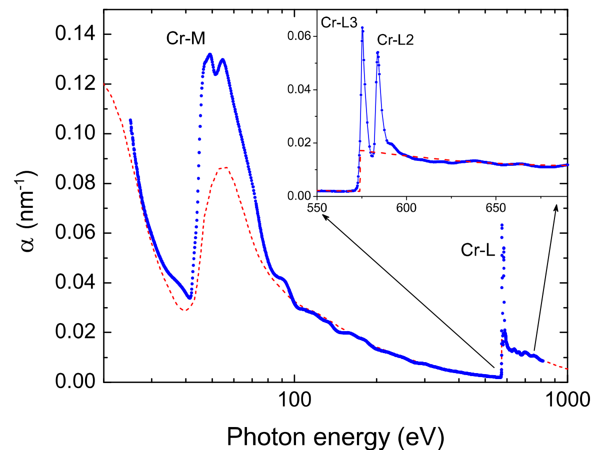

FIG. 12. The Cr linear absorption coefficient α (linear scale) vs. photon energy (log scale) determined by our transmission measurements (blue circles) from 25 eV to 813 eV. Values calculated from tabulated data (Ref. 16) (red dash line) are plotted for comparison. The inset displays details of the Cr-L edge region with the photon energy on a linear scale.

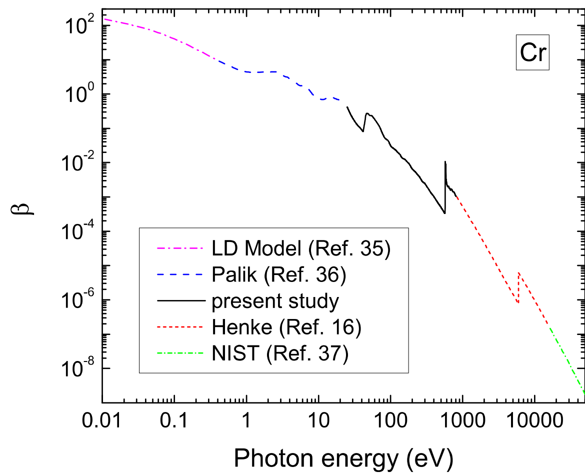

FIG. 13. Compilation of theoretical and experimental β values of Cr used to calculate δ [Eq. (5)]: Lorentz-Drude (LD) model[35] (magenta dash dotted line); experimental data from Ref. 36 (blue dashed line); experimental data from the present study (black solid line); and tabulated data from Refs. 16 and 17 (red short dashed line) and from Ref. 37 (green short dashed dot).

Lorentz-Drude model proposed by Rakić *et al.* in the spectral range of 1×10^{-4} eV to 0.41 eV (Ref. 35); (ii) experimental data from Palik in the spectral range of 0.42 eV to 23 eV (Ref. 36); (iii) experimental data from the present study [Eq. (4)] in the spectral range of 25 eV to 813 eV; (iv) tabulated data from Ref. 16 in the spectral range of 838 eV to 16046 eV; and (v) tabulated data from the National Institute of Standards and Technology (NIST) in the spectral region 16463 eV to 432945 eV (Ref. 37). One can see in Fig. 13 that there is good continuity between all sets of data.

Figure 14 shows the δ values calculated by the Kramers-Kronig relation [Eq. (5)] with the compilation of β values described above (Fig. 13). The improved accuracy and resolution (fine structure) in the β values (compared to tabulated data[16]) in the Cr-L and Cr-M edge regions result in important differences in the δ values. It is interesting to notice that these differences remain significant, even quite far from the edges. For instance, at E = 91.48 eV (which is the photon energy region of operation for applications such as photolithography, solar physics, and synchrotron instrumentation, which employ Cr-coated optics), the δ and β values of Cr (0.0749 and 0.04393, respectively) are more than 10% higher than the tabulated values in Ref. 16 (0.067548 and 0.038883, respectively).

In order to test the accuracy of the β dataset that we use in the Kramers-Kronig relation [Eq. (5)], we have calculated the total number of electrons (N_{eff}) effective in the absorption process[38]

$$N_{eff} = \frac{4m\epsilon_0}{\pi n_a e^2}\int_0^{\infty} E'\beta(E')\,dE'. \quad (6)$$

If the β dataset is fully consistent, then we should have

$$N_{eff} = Z^*, \quad (7)$$

which is the so-called f-sum rule (ref Smith), and here, Z* represents the atomic number Z, corrected by the relativistic effect[16]

$$Z^* = Z - (Z/82.5)^{2.37}. \quad (8)$$

Thus, N_{eff} can be used to check the consistency and accuracy of the β values. For Cr atoms, Eq. (8) gives Z* = 23.95. With the set of β values described above (see Fig. 13), including our new experimental data in the range 25 eV–813 eV, we obtain N_{eff} = 23 from Eq. (6). If we replace our experimental data in the range 25 eV–813 eV by previous tabulated data (Ref. 16), we obtain N_{eff} = 21.39.

We estimated the uncertainty on the determination of absorption values by our method to be within ±2%, corresponding to a deviation of less than 0.28 electrons in N_{eff}. Thus, the accuracy and consistency of the entire optical constant dataset for Cr are improved by the experimental data from the present study. There is still a residual difference equivalent to 0.95 electrons between N_{eff} and Z* which we believe to be due to errors in the tabulated values at low energies (below 25 eV). For those interested in examining

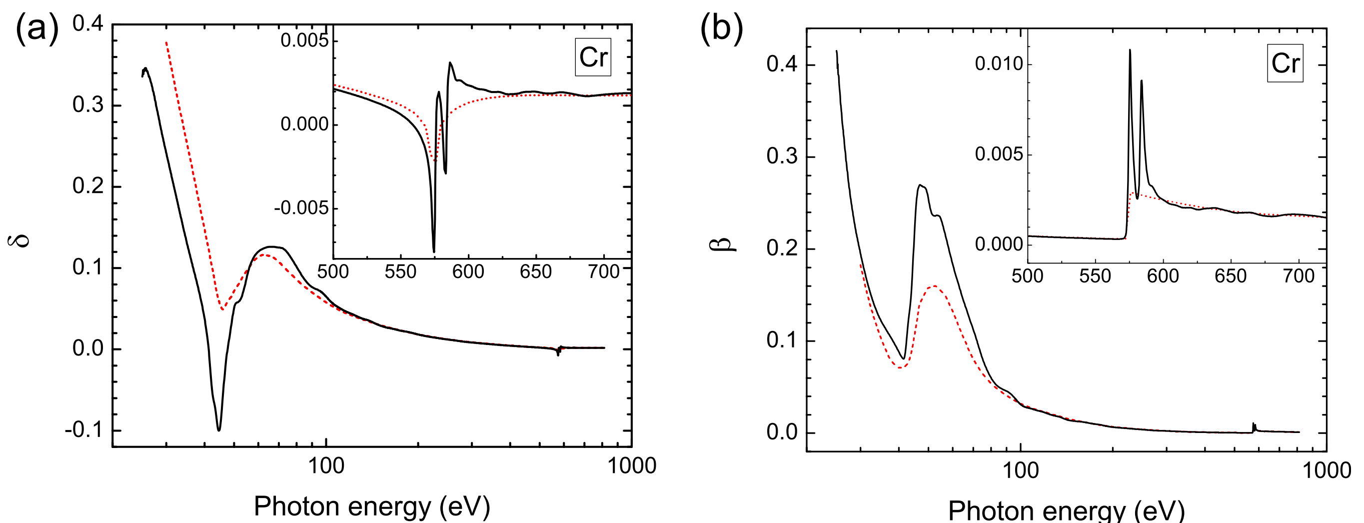

FIG. 14. δ and β values for Cr determined in this work (black solid line) in the spectral range of 25 eV to 813 eV (log scale) compared with previous tabulated data (Ref. 16) (red dashed line). The inset shows details of the Cr-L edge region with the photon energy on a linear scale.

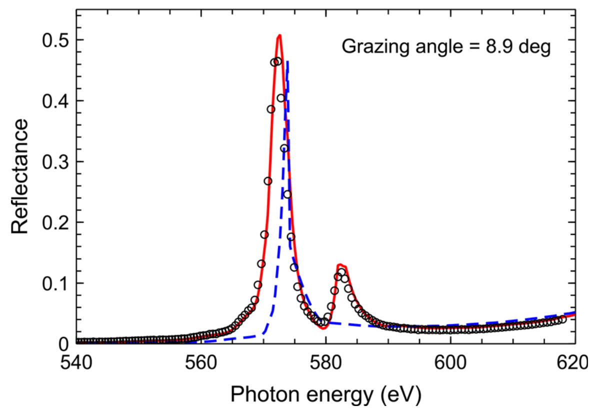

FIG. 15. Cr/B_4C multilayer reflectance is plotted vs. photon energy around the Cr-L edge: experimental data (circles), simulation using Cr optical constants from this study (red solid line), and simulation using tabulated Cr optical constants from Ref. 16 (blue dashed line). The number of periods is 35, and the period thickness is 6.68 nm. The grazing angle is 8.9°.

the accuracy of the β-value dataset in a particular photon energy "window," a method has been proposed in Ref. 39, based on the use of window functions in sum rules.

Additionally, we have verified that our new Cr optical constants are consistent with experimental results on Cr-based multilayer reflectance. Specifically, we have simulated the reflectance spectra of a Cr/B4C multilayer that was measured at ALS beamline 6.3.2 around the Cr-L edge.[6] The model used for the simulation is also given in Ref. 6. Figure 15 shows that the simulation with the new Cr optical constants is in very good agreement with the experimental data, whereas the previously tabulated Cr optical constants (Ref. 16) did not permit to reproduce accurately the multilayer reflectance in this spectral range. Figure 15 represents a definite validation of the newly determined Cr optical constants in the L-edge photon energy region.

VII. CONCLUSION

We have determined a new set of soft x-ray optical constants (δ and β) for sputtered Cr thin films, via absolute photoabsorption measurements. The new values include, for the first time, the fine structure in the M- and L-edge photon energy regions. As part of this work, the composition, density, and aging of Cr thin films were studied. The measured density of our Cr films is consistent with the tabulated value of 7.19 g/cm^3. No contaminant was detected in the films, apart from a nanometric oxide surface layer which remains stable after up to 4 years of aging.

Eight freestanding Cr thin films with a thickness ranging from 20 nm to 300 nm were successfully produced and characterized. The Cr absorption coefficient β was calculated from the transmittance measured on these samples. A model was proposed to take into account the spectral contamination of the source and was successfully applied in the Cr-L edge region. This model allows us to correct the value of the absorption coefficient from the effect of spectral contamination. It can also be used to characterize the spectral purity of the source.

A compilation of β values at photon energies from 10^{-4} eV to 4.3×10^5 eV was produced in order to determine δ by the Kramers-Kronig relation. This compilation includes the experimental values from this work and theoretical or tabulated values at lower and higher energies. We demonstrated the improved accuracy of the new Cr optical constants via the f-sum rule test and by simulating the experimental reflectance of a Cr/B_4C multilayer in the Cr-L edge region.

The newly determined Cr optical constants will be disseminated in the scientific community and will enable simulations of Cr-based optics in the EUV and soft x-ray range with significantly improved accuracy.

ACKNOWLEDGMENTS

This work was supported by a STSM Grant from COST Action MP1203 and by the Jean d'Alembert fellowship program from Université Paris-Saclay. This work was performed under the auspices of the U.S. Department of Energy by Lawrence Livermore National Laboratory under Contract No. DE-AC52-07NA27344.

[1]F. Schäfers, H.-C. Mertins, F. Schmolla, I. Packe, N. N. Salashchenko, and E. A. Shamov, "Cr/Sc multilayers for the soft-x-ray range," Appl. Opt. **37**, 719–728 (1998).
[2]H. Stollberg, S. Yulin, P. A. C. Takman, and H. M. Hertz, "High-reflectivity Cr/Sc multilayer condenser for compact soft x-ray microscopy," Rev. Sci. Instrum. **77**, 123101 (2006).
[3]A. Guggenmos, R. Rauhut, M. Hofstetter, S. Hertrich, B. Nickel, J. Schmidt, E. M. Gullikson, M. Seibald, W. Schnick, and U. Kleineberg, "Aperiodic CrSc multilayer mirrors for attosecond water window pulses," Opt. Express **21**, 21728–21740 (2013).
[4]S. de Rossi, C. Bourassin-Bouchet, E. Meltchakov, A. Giglia, S. Nannarone, and F. Delmotte, "Phase measurement of soft x-ray multilayer mirrors," Opt. Lett. **40**, 4412–4415 (2015).
[5]M. Prasciolu, A. F. G. Leontowich, K. R. Beyerlein, and S. Bajt, "Thermal stability studies of short period Sc/Cr and $Sc/B_4C/Cr$ multilayers," Appl. Opt. **53**, 2126–2135 (2014).
[6]C. Burcklen, R. Soufli, D. Dennetiere, F. Polack, B. Capitanio, E. Gullikson, E. Meltchakov, M. Thomasset, A. Jérome, S. de Rossi, and F. Delmotte, "Cr/B_4C multilayer mirrors: Study of interfaces and X-ray reflectance," J. Appl. Phys. **119**, 125307 (2016).
[7]E. M. Gullikson, F. Salmassi, A. L. Aquila, and F. Dollar, see http://escholarship.org/uc/item/8hv7q0hj for "Progress in short period multilayer coatings for water window applications," paper presented at the 8th International Conference on the Physics of X-Ray Multilayer Structures (PXRMS), oral presentation, Sapporo, Japan (2006).
[8]Q. Huang, J. Fei, Y. Liu, P. Li, M. Wen, C. Xie, P. Jonnard, A. Giglia, Z. Zhang, K. Wang, and Z. Wang, "High reflectance Cr/V multilayer with B_4C barrier layer for water window wavelength region," Opt. Lett. **41**, 701–704 (2016).
[9]N. Ghafoor, P. O. Å. Persson, J. Birch, F. Eriksson, and F. Schäfers, "Interface engineered ultrashort period Cr-Ti multilayers as high reflectance mirrors and polarizers for soft x rays of lambda = 2.74 nm wavelength," Appl. Opt. **45**, 137–143 (2006).
[10]M. Niibe, M. Tsukamoto, T. Iizuka, A. Miyake, Y. Watanabe, and Y. Fukuda, "Fabrication and evaluation of Cr-C multilayer mirrors for soft x rays," Proc. SPIE **1720**, 208–216 (1992); M. Wen, L. Jiang, Z. Zhang, Q. Huang, Z. Wang, R. She, H. Feng, and H. Wang, "High reflectance Cr/C multilayer at 250 eV for soft X-ray polarimetry," Thin Solid Films **592**, 262–265 (2015).
[11]S. A. Yulin, F. Schaefers, T. Feigl, and N. Kaiser, "Enhanced reflectivity and stability of Sc/Si multilayers," Proc. SPIE **5193**, 155–163 (2004).
[12]Z. Guojing, Y. Pei-yang, and L. Ted, "Cr absorber mask for extreme-ultraviolet lithography," Proc. SPIE **4186**, 774–780 (2001).
[13]D. Martínez-Galarce, R. Soufli, D. L. Windt, M. Bruner, E. Gullikson, S. Khatri, E. Spiller, J. C. Robinson, S. Baker, and E. Prast,

"Multisegmented, multilayer-coated mirrors for the Solar Ultraviolet Imager," Opt. Eng. **52**, 095102 (2013).
[14]R. Soufli, J. C. Robinson, M. Fernández-Perea, E. Spiller, N. F. Brejnholt, M.-A. Descalle, M. J. Pivovaroff, and E. M. Gullikson, "Recent advances in reflective optics for EUV/x-ray laser sources," in *X-Ray Lasers 2014: Proceedings of the 14th International Conference on X-Ray Lasers*, edited by , J. Rocca, C. Menoni, and M. Marconi (Springer, 2015), Vol. 169, p. 331.
[15]D. E. Graessle, R. Soufli, A. J. Nelson, C. L. Evans, A. L. Aquila, E. M. Gullikson, R. L. Blake, and A. J. Burek, "Iridium optical constants from synchrotron reflectance measurements over 0.05- to -12 keV x-ray energies," Proc. SPIE **5538**, 72–83 (2004).
[16]B. Henke, E. Gullikson, and J. Davis, "X-ray interactions: Photoabsorption, scattering, transmission, and reflection at E = 50–30000 eV, Z = 1–92," At. Data Nucl. Data Tables **54**, 181–342 (1993).
[17]See http://henke.lbl.gov/optical_constants/ for an updated version of Ref. 16.
[18]J. Gautier, F. Delmotte, M. Roulliay, F. Bridou, M.-F. Ravet, and A. Jérome, "Study of normal incidence of three-component multilayer mirrors in the range 20–40 nm," Appl. Opt. **44**, 384–390 (2005).
[19]A. Hardouin, F. Delmotte, M. F. Ravet, F. Bridou, A. Jérôme, F. Varnière, C. Montcalm, S. Hedacq, E. Gullikson, and P. Aubert, "Experimental study of Cr/Sc multilayer mirrors for the nitrogen Kalpha-emission line," J. Vac. Sci. Technol. A **26**, 333 (2008).
[20]J. H. Underwood and E. M. Gullikson, "High-resolution, high-flux, user friendly VLS beamline at the ALS for the 50-1300 eV energy region," J. Electron Spectrosc. Relat. Phenom. **92**, 265–272 (1998).
[21]E. M. Gullikson, S. Mrowka, and B. B. Kaufmann, "Recent developments in EUV reflectometry at the advanced light source," Proc. SPIE **4343**, 363–373 (2001).
[22]D. L. Windt, "IMD - Software for modeling the optical properties of multilayer films," Comput. Phys. **12**, 360–370 (1998).
[23]C. Cohen, J. A. Davies, A. V. Drigo, and T. E. Jackman, "Intercomparison of absolute standards for RBS studies," Nucl. Instrum. Methods Phys. Res. **218**, 147–148 (1983).
[24]Y. Sakisaka, H. Kato, and M. Onchi, "Oxygen chemisorption and initial oxidation of Cr(110)," Surf. Sci. **120**, 150–170 (1982).
[25]R. Peter, I. Saric, I. K. Piltaver, I. J. Badovinac, and M. Petravic, "Oxide formation on chromium metal surfaces by low-energy oxygen implantation at room temperature," Thin Solid Films **636**, 225–231 (2017).
[26]M. Mayer, "Improved physics in SIMNRA 7," Nucl. Instrum. Methods Phys. Res., Sect. B **332**, 176–180 (2014).
[27]W. K. Chu, J. W. Mayer, and M.-A. Nicolet, *Backscattering Spectrometry* (Academic Press, New York, 1978), ISBN: 0-12-173850-7.
[28]*CRC Handbook of Chemistry and Physics*, edited by D. R. Lide (CRC Press, Boca Raton, FL, 2005), pp. 4–9.
[29]R. Soufli and E. M. Gullikson, "Reflectance measurements on clean surfaces for the determination of optical constants of silicon in the extreme ultraviolet–soft-x-ray region," Appl. Opt. **36**, 5499–5507 (1997).
[30]T. Schedel-Niedrig, T. Neisius, C. T. Simmons, and K. Köhler, "X-ray absorption spectroscopy of small chromium oxide particles (Cr_2O_3, CrO_2) supported on titanium dioxide," Langmuir **12**, 6377–6381 (1996).
[31]J. G. Chen, B. Frühberger, and M. L. Colaianni, "Near-edge x-ray absorption fine structure characterization of compositions and reactivities of transition metal oxides," J. Vac. Sci. Technol. A **14**, 1668 (1996).
[32]R. Haensel, C. Kunz, T. Sasaki, and B. Sonntag, "Absorption measurements of copper, silver, tin, gold, and bismuth in the far ultraviolet," Appl. Opt. **7**, 301–306 (1968).
[33]B. Sonntag, R. Haensel, and C. Kunz, "Optical absorption measurements of the transition metals Ti, V, Cr, Mn, Fe, Co, Ni in the region of 3p electron transitions," Solid State Commun. **7**, 597–599 (1969).
[34]M. Altarelli, D. L. Dexter, H. M. Nussenzveig, and D. Y. Smith, "Superconvergence and sum rules for the optical constants," Phys. Rev. B **6**, 4502–4509 (1972).
[35]A. D. Rakić, A. B. Djurišić, J. M. Elazar, and M. L. Majewski, "Optical properties of metallic films for vertical-cavity optoelectronic devices," Appl. Opt. **37**, 5271–5283 (1998).
[36]*Handbook of Optical Constants of Solids*, edited by E. D. Palik (Academic Press, Boston, 1998), pp. 374–385.
[37]C. T. Chantler, "Theoretical form factor, attenuation and scattering tabulation for Z=1-92 from E=1-10 eV to E=0.4-1.0 MeV," J. Phys. Chem. Ref. Data **24**, 71–643 (1995); See http://physics.nist.gov/ffast for an updated version of X-ray Form Factor, Attenuation and Scattering Tables (Version 2.1) (National Institute of Standards and Technology, Gaithersburg, MD, 2005).
[38]D. Y. Smith and E. Shiles, "Finite-energy f-sum rules for valence electrons," Phys. Rev. B **17**, 4689–4694 (1978).
[39]L. V. Rodríguez-de Marcos, J. A. Méndez, and J. I. Larruquert, "Tuning sum rules with window functions for optical constant evaluation," J. Opt. **18**, 075606 (2016).